

Provided for non-commercial research and education use.
Not for reproduction, distribution or commercial use.



This article appeared in a journal published by Elsevier. The attached copy is furnished to the author for internal non-commercial research and education use, including for instruction at the authors institution and sharing with colleagues.

Other uses, including reproduction and distribution, or selling or licensing copies, or posting to personal, institutional or third party websites are prohibited.

In most cases authors are permitted to post their version of the article (e.g. in Word or Tex form) to their personal website or institutional repository. Authors requiring further information regarding Elsevier's archiving and manuscript policies are encouraged to visit:

<http://www.elsevier.com/copyright>



Contents lists available at ScienceDirect

Journal of Power Sources

journal homepage: www.elsevier.com/locate/jpowsour

A study of the electrochemical processes in lithium–sulphur cells by impedance spectroscopy[☆]

V.S. Kolosnitsyn, E.V. Kuzmina, E.V. Karaseva*, S.E. Mochalov

Institution of the Russian Academy of Sciences Institute of Organic Chemistry of Ufa Scientific Center of the Russian Academy of Sciences, Laboratory of Electrochemistry, 71, pr. Oktyabrya, Ufa, Bashkortostan, 450054, Russia

ARTICLE INFO

Article history:

Received 28 June 2010

Received in revised form 12 August 2010

Accepted 29 August 2010

Available online 6 September 2010

Keywords:

Lithium–sulphur cells

AC impedance

Cycling

Lithium polysulphides

ABSTRACT

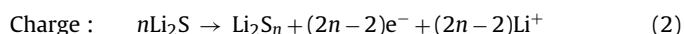
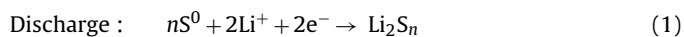
The changes in the properties of lithium–sulphur cell components (electrolyte, sulphur and lithium electrodes) during cycling are studied by AC impedance spectroscopy. It is shown that during the charge and discharge of lithium–sulphur cells the conductivity of the electrolyte is changed. We believe that the observed changes in the electrolyte conductivity can be explained by the formation of soluble lithium polysulphides by electrochemical reactions. The properties of the electrolyte significantly influence the rate of the electrochemical processes which occur both on the sulphur and lithium electrodes in lithium–sulphur cells.

© 2010 Elsevier B.V. All rights reserved.

1. Introduction

The lithium–sulphur electrochemical system has a number of advantages over lithium-ion batteries. These advantages include high energy density, low cost and the availability of electrode materials. However, so far lithium–sulphur batteries have not found any commercial application because of a series of unsolved problems. A significant problem has been rapid capacity fade during cycling [1–4].

The properties of the lithium–sulphur battery are determined by specific electrochemical, physicochemical and chemical processes which occur in lithium–sulphur cells during discharge and charge. Lithium polysulphides (Li_2S_n), generated during the electrochemical discharge (1) and charge (2), readily dissolve in most aprotic solvents.



Dissolved lithium polysulphides produce changes in the physicochemical properties of electrolyte; decreasing conductivity and increasing viscosity [5,6]. Changes to the properties of electrolytes

can considerably influence the electrochemical processes which occur in lithium–sulphur cells during cycling.

The current work explores the influence of lithium polysulphides on the AC impedance diagrams of the lithium–sulphur cells as a function of the state of charge.

2. Experimental

The sulphur electrodes consisted of 70 wt.% sublimed sulphur (99.5%, Acros organics), 10 wt.% Ketjenblack EC-600 JD (surface area $\approx 1400 \text{ m}^2 \text{ g}^{-1}$ (BET), Akzo Nobel Polymer Chemicals LLC), and 20 wt.% poly(ethylene oxide) (PEO, Mw 4×10^6 , Sigma–Aldrich). Sulphur, Ketjenblack EC-600 JD powder and PEO were mixed in a grinding mill (Homogenising system MICROTRON MB 550 Kinematica ID) for 60 s at high speed, this procedure was carried out 10 times. The acetonitrile (99.8%, anhydrous, Aldrich) was poured into the mixed powder of sulphur, Ketjenblack EC-600 JD and PEO and then stirred for 48 h to make a homogenous slurry. The slurry was coated on to carbon-coated Al foil and dried in the air at 50°C for 2 h. The resulting electrode film was pressed with a twin roller, cut into a disc and dried under vacuum at 60°C for 24 h. The total thickness of electrode layer was approximately $20 \mu\text{m}$, the loading level of sulphur corresponded to 2 mAh cm^{-2} .

Lithium metal foil (98+ wt.%, FMC Corp., USA) with the thickness of $78 \pm 1 \mu\text{m}$ and $70 \pm 1 \mu\text{m}$ was used as the auxiliary and reference electrodes, respectively. 1 M LiClO_4 (99.99%, battery grade, Sigma–Aldrich) in sulfolane (anhydrous, Degussa Stanlow Ltd.) was used as the electrolyte.

[☆] This work was presented on the 214th Meeting of the ECS, Honolulu, HI, October 12–17, 2008, Volume 16, Issue 29, p. 1238.

* Corresponding author. Tel.: +7 347 2355800; fax: +7 347 2355800.

E-mail addresses: kolos@anrb.ru (V.S. Kolosnitsyn), kuzmina@anrb.ru (E.V. Kuzmina), karaseva@anrb.ru, karaseva@oxisenergy.com (E.V. Karaseva), elchem@anrb.ru (S.E. Mochalov).

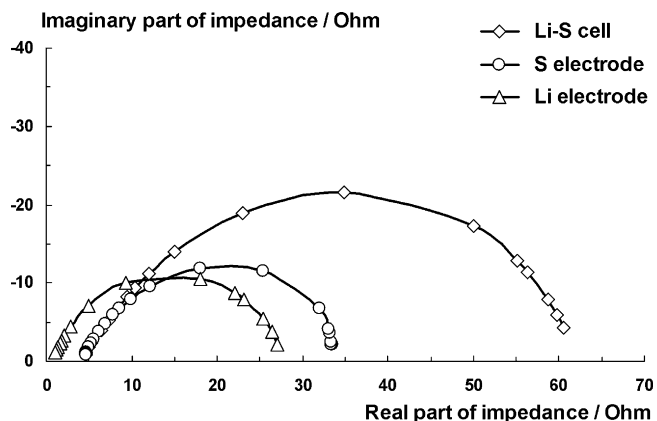


Fig. 1. The impedance diagrams of a freshly prepared three-electrode lithium–sulphur cell, a lithium electrode and a sulphur electrode. The lithium and sulphur electrode data were obtained relative to the reference electrode.

In this study we used two-electrode and three-electrode sealed stainless-steel cells with plane-parallel electrodes. Porous polypropylene Celgard 3501 (thickness $25 \pm 1 \mu\text{m}$, porosity 55%, Celgard LLC) was used alone as the separator ($d=2.85 \text{ cm}$, area = 6.38 cm^2) in two-electrode cells and together with non-woven polypropylene in three-electrode cells (the total thickness of the Celgard 3501 and polypropylene was $100 \pm 5 \mu\text{m}$, $d=2.85 \text{ cm}$, area = 6.38 cm^2).

The two-electrode lithium–sulphur cells were assembled by stacking a lithium foil ($d=2.55 \text{ cm}$, area = 5.10 cm^2), a Celgard 3501 polypropylene separator containing 1 M LiClO_4 in sulfolane and a sulphur electrode ($d=2.85 \text{ cm}$, area = 6.38 cm^2).

The three-electrode lithium–sulphur cells were assembled in a similar fashion, however a reference electrode (area $\sim 6 \text{ mm}^2$) was placed between the Celgard 3501 polypropylene separator and the non-woven polypropylene separator such that it did not shield the working (sulphur, $d=1.07 \text{ cm}$, area = 3.60 cm^2) and auxiliary (lithium, $d=2.85 \text{ cm}$, area = 6.38 cm^2) electrodes.

Electrolyte preparation, lithium electrode manufacture and lithium–sulphur cell assembly were all carried out in an argon filled glove box (M. Braun GmbH, Germany). The concentration of water and oxygen was maintained below 1 ppm.

The main investigations were carried out in the two-electrode cells because they better simulate the real lithium–sulphur batteries.

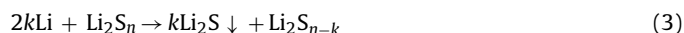
The experiment was carried out in the following way. The charge and discharge performances of the assembled cells were investigated with a PG12–100 potentiostat between 1.5 V and 2.8 V. The current density was 0.2 mA cm^{-2} . A sinusoidal current signal was added to the direct current to measure the AC impedance of the cell. The amplitude of the current signal was selected in order that the corresponding voltage amplitude was no more than 4 mV. The response was analysed using a Solatron 1250 frequency response analyser. The AC impedance was measured over a frequency range of 1 Hz to 65 kHz. A sweep was automatically performed 10–30 times at selected states of charge. The data was analysed using a model circuit derived by the ZView (Scribner Associates, Inc.) electrochemical analysis program [7].

3. Results and discussion

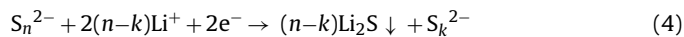
Fig. 1 shows the impedance diagram of the three-electrode lithium–sulphur cell in its pre-cycled state; as well as and the impedance diagrams of its lithium and sulphur electrodes. The impedances of the lithium and sulphur electrodes were measured relative to a reference electrode; hence the need for a

three-electrode cell. The impedance diagrams are semicircles with their centres below the X-axis in the studied frequency range. The impedance diagram of the lithium–sulphur cell is the sum of the impedance diagrams of the lithium and sulphur electrodes. The impedance diagrams associated with the sulphur and lithium electrodes are similar and located within the tested frequency range. This fact provides evidence that the impedance diagrams of the lithium and sulphur electrodes reflect the behaviour of similar objects. It is likely that the impedance diagram of the lithium–sulphur cell is related to the surface layers which are formed on the sulphur and lithium electrodes.

It is well known that the composition of the surface layer on lithium electrode, or solid–electrolyte interphase (SEI), depends on the composition of the electrolyte system. Before cycling and during several initial charge–discharge cycles the primary passivating film on the surface of lithium electrode mainly consists of the products from the reaction between lithium and the components of electrolyte systems. During the cycling of lithium–sulphur cells the composition of the SEI on the surface of the lithium electrodes are changing because of the inclusion of lithium sulphide (Li_2S) [8,9]. The lithium sulphide is formed by the interfacial reaction between lithium and lithium polysulphides dissolved in the electrolyte (3). The lithium polysulphides are generated during the discharge and charge of the lithium–sulphur cells as a result of the reduction of sulphur and the oxidation of lithium sulphide [10,11].



The properties of the sulphur electrode before and during cycling are different [12]. It is well known that the sulphur is sparingly soluble in most aprotic solvents [13]. Nevertheless some sulphur dissolves in the electrolyte and is then it adsorbed onto the surface of the carbon particles. Thus before cycling there is a layer of adsorbed sulphur on the surface of carbon particles. At this electrode, lithium sulphide is precipitated during discharge (4), and sulphur–during charge (5):



The changes in the composition of the SEI layer on the lithium electrode, and the formation of a layer of solid products on the surface of the sulphur electrode, lead to significant changes in the impedance responses as the cell cycles (Figs. 2–4).

During the first discharge the diameter of the semicircle in the impedance diagram decreases (Fig. 2a). A qualitative change of the impedance response shape is also observed when the cell reaches a state corresponding to the middle of the low-voltage plateau (Fig. 2b). The low-frequency feature changes into a straight line with a slope of about 45° .

The dependences of the impedance diagrams for the lithium–sulphur cell on the depth of discharge and charge are shown in Figs. 3 and 4, respectively. It should be noted that the shapes of the impedance plots during the first discharge cycle (Fig. 2a) and during the subsequent cycles (Figs. 3a and 4a) are different. The impedance diagram (Figs. 3a and 4a) consists of two regions. The shape of the high-frequency region does not depend on the state of charge, while the shape of the low-frequency region does depend on the state of charge. At the initial and final stages of discharge (Fig. 3a) and charge (Fig. 4a), the low-frequency regions of the impedance diagram are seen to be characteristic of diffusion limiting processes, whereas at intermediate stages of charge and discharge, the shape of the low-frequency impedance diagram is an arc from a single semicircle.

For analysis we propose two equivalent circuits, corresponding to a fully charged or discharged cell (Fig. 5a) and a cell in an intermediate state (Fig. 5b).

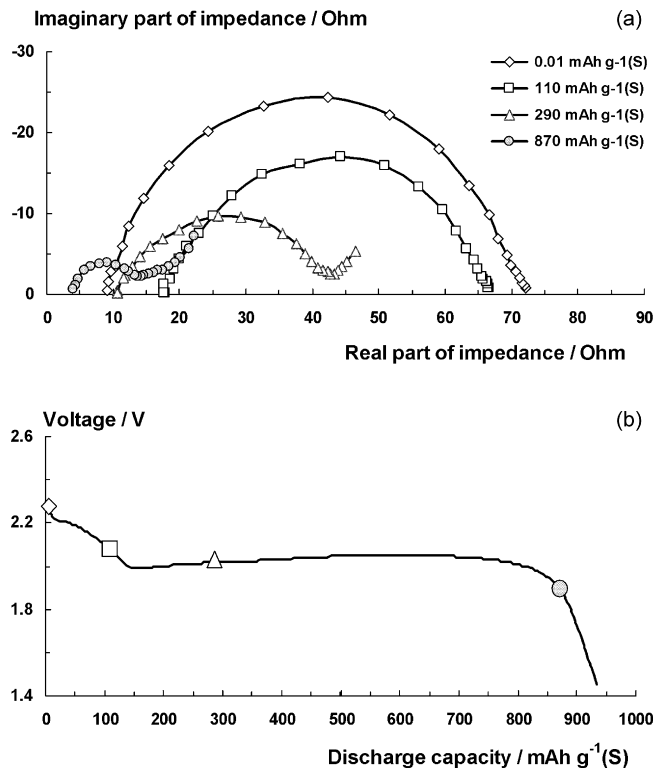


Fig. 2. The changes in the impedance response as a function of the depth of discharge of a two-electrode lithium–sulphur cell during the first discharge cycle (a) and the discharge curve of a two-electrode lithium–sulphur cell (b). $i = 0.2 \text{ mA cm}^{-2}$; room temperature; 1st cycle. The markers on the discharge curve correspond to the presented impedance diagrams.

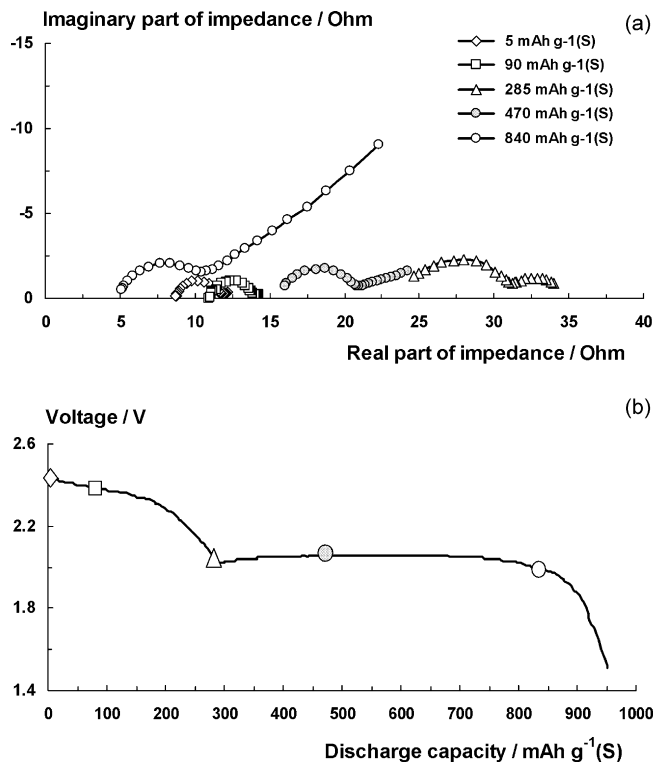


Fig. 3. The changes in the impedance response as a function of the depth of discharge of a two-electrode lithium–sulphur cell during the second discharge cycle (a) and the discharge curve of a two-electrode lithium–sulphur cell (b). $i = 0.2 \text{ mA cm}^{-2}$; room temperature; 2nd cycle. The markers on the discharge curve correspond to the presented impedance diagrams.

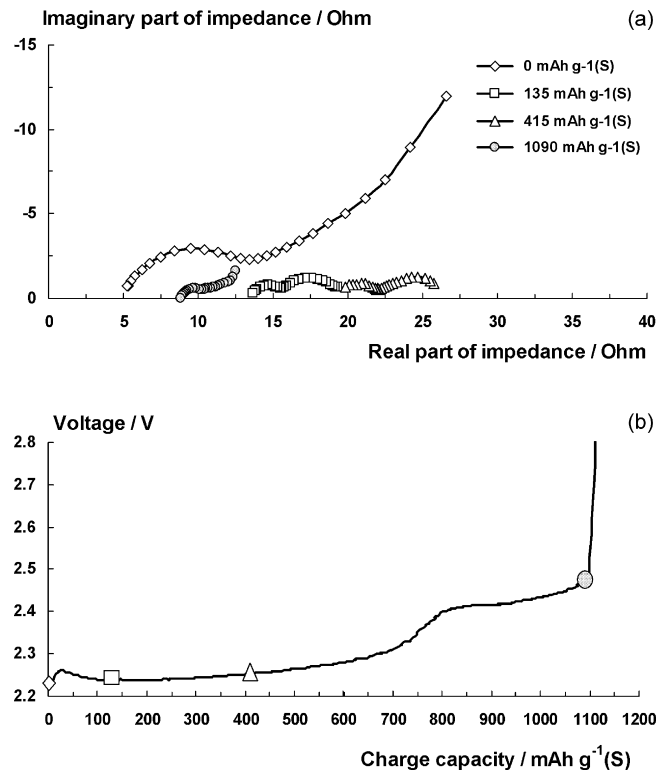


Fig. 4. The changes in the impedance response as a function of the depth of charge of a two-electrode lithium–sulphur cell during the third charge cycle (a) and the charge curve of a two-electrode lithium–sulphur cell (b). $i = 0.2 \text{ mA cm}^{-2}$; room temperature; 3rd cycle. The markers on the charge curve correspond to the presented impedance diagrams.

The electrolyte resistance (R_{el}) is determined by extrapolation of the Nyquist plot to an infinitely large frequency.

We assume that the high-frequency semicircle defines the overall impedance of the surface layers on both electrodes. Therefore, the resistance of the surface layers (R_{sl}) is the sum of resistances of the surface layers on the both electrodes. The resistance of the surface layers is determined from the diameter of the high-frequency semicircle. The constant-phase element CPE_{sl} is a distributed capacitance of the surface layers.

The low-frequency region of the impedance diagrams describes the electrochemical reactions on the sulphur electrodes [9,11,12,14]. The resistance R_{er} is determined by the rate of

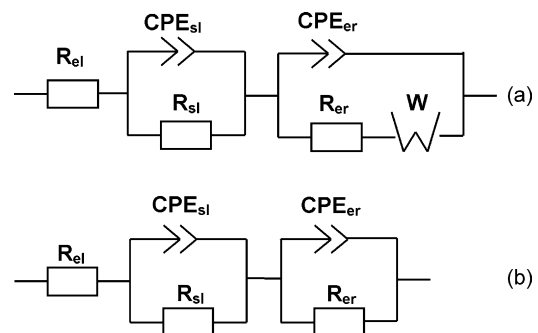


Fig. 5. The equivalent circuits corresponding to a fully charged or discharged lithium–sulphur cell (a) and a lithium–sulphur cell in an intermediate state (b). R_{el} : resistance of electrolyte; R_{sl} : total resistance of the surface layers on the sulphur and lithium electrodes; CPE_{sl} : distributed capacitance of the surface layers of both the sulphur and lithium electrodes; R_{er} : resistance to charge transfer on the sulphur electrode; CPE_{er} : a double layer capacitance distributed on the surface of the pores in the sulphur electrode; W : the Warburg impedance.

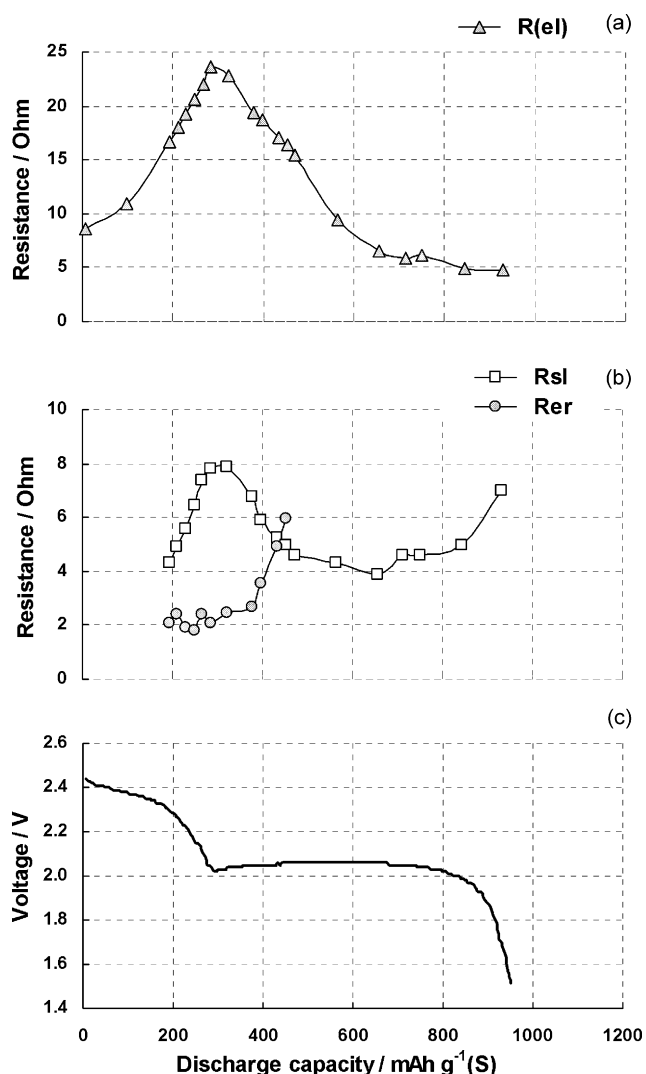


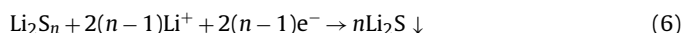
Fig. 6. The dependences of the electrolyte resistance (R_{el} , a), the resistance of the surface layers (R_{sl} , b) and the resistance to charge transfer (R_{er} , b) on the depth of discharge of the two-electrode lithium–sulphur cell and the discharge curve of the two-electrode lithium–sulphur cell (c). $i = 0.2 \text{ mA cm}^{-2}$; room temperature; 2nd cycle.

electrochemical reaction on the sulphur electrode. These reactions can occur with diffusion limitations that are described by the Warburg impedance (W). The CPE_{er} represents a double layer capacitance formed on the surface of the sulphur electrode.

3.1. Discharge of lithium–sulphur cell

During a cell discharge the electrolyte resistance (R_{el}) has a maximum (Fig. 6a) which coincides with the “potential dip” between high-voltage and low-voltage plateaus on a cell discharge curve (Fig. 6c). This maximum corresponds to the peak in concentration of the lithium polysulphides (Li_2S_n) in the electrolyte solution. In the past we have determined that the viscosity of the lithium polysulphides solutions increased with its concentration. Thus it may be concluded that the increase in electrolyte resistance is caused by the increase in the electrolyte viscosity; itself due to lithium polysulphides accumulation within the bulk of the electrolyte. The subsequent decrease of electrolyte resistance is related to the decrease in the concentration of lithium polysulphides as a result of their reduction during the further discharge

of the lithium–sulphur cell (6):



The total resistance of the surface layers on both the sulphur and lithium electrodes (R_{sl}) is an S-type curve (Fig. 6b) where the maximum resistance coincides with the maximum resistance of the similar electrolyte resistance curve (R_{el} , Fig. 6a). The measurements carried out using a three-electrode cell show that the maxima in R_{el} are observed for both lithium and sulphur electrodes. It should be noted that these maxima are less clearly defined in the measurements made using the three-electrode cell than for those in the two-electrode cell.

As mentioned above, the passivating surface film is generated in lithium polysulphides solutions because of the interfacial reaction between lithium and lithium polysulphides (3). This film mainly consists of lithium sulphide. As long as Li_2S is known to be non-conductive, the conductivity of the passivating film is likely to be dependant on the conductivity of the electrolyte present in the pores of the Li_2S film. If this hypothesis is correct, then the reason for the maximum, present in the resistance curve (R_{sl} , Fig. 6b), is the dependence of the surface film morphology on the depth of cell discharge (and hence lithium polysulphides concentration). Although it may also be due to the increase in electrolyte viscosity, during the first step of the lithium–sulphur cell discharge.

The thickness of the lithium sulphide film on the surface of the lithium electrode is determined by the rates of formation and dissolution of Li_2S . The concentration of lithium polysulphides in the electrolyte gradually decreases during discharge. As long-chain lithium polysulphides are involved in the re-dissolution of the Li_2S film, their disappearance, together with the continued production of Li_2S results in an increase in film thickness. Therefore the increase in the resistance of the surface layers (R_{sl} , Fig. 6b) is caused by the increase in thickness of the passivating film. The rate at which the film dissolves decreases as the concentration of long-chain lithium polysulphides in the electrolyte decreases during the discharge process.

The maximum in the resistance of the surface layer on the sulphur electrode (R_{sl} , Fig. 6b) corresponds to the maximum of the electrolyte resistance (R_{el} , Fig. 6a) and it is caused by transport difficulties due to the accumulation of long-chain lithium polysulphides in the micropores of the electrode.

The resistance to charge transfer on the sulphur electrode (R_{er}) can be seen to be constant until approximately half way through the discharge curve, and then it rapidly increases (Fig. 6b). We were unable to calculate R_{er} at deep states of discharge due to the rapid increase in the semicircle radius corresponding to the electrochemical reactions. Only a small part of the low-frequency arc was observed in the measurable frequency range. This curve could be interpreted, either as the beginning of a diffusion branch or as the beginning of a semicircle. Therefore, it was impossible to treat this as part of the impedance diagram. To solve this problem, we suggest the frequency range could be extended by one or more orders of magnitude into the low-frequency area. However, in this case the time period of the AC current used to measure the impedance spectrum is comparable with the time required for full discharge of the cell.

It is more likely that the initial low value of R_{er} is caused by the high rate of the electrochemical reduction of sulphur. The increase of R_{er} indicates the decrease of the rate of the reduction of lithium polysulphides (4). This is due to the decrease of average polysulphide degree as the cell discharges.

3.2. Charge of lithium–sulphur cell

The form of the curves showing the dependence of electrolyte resistance on the depth of charge (R_{el} , Fig. 7a) and the depth of

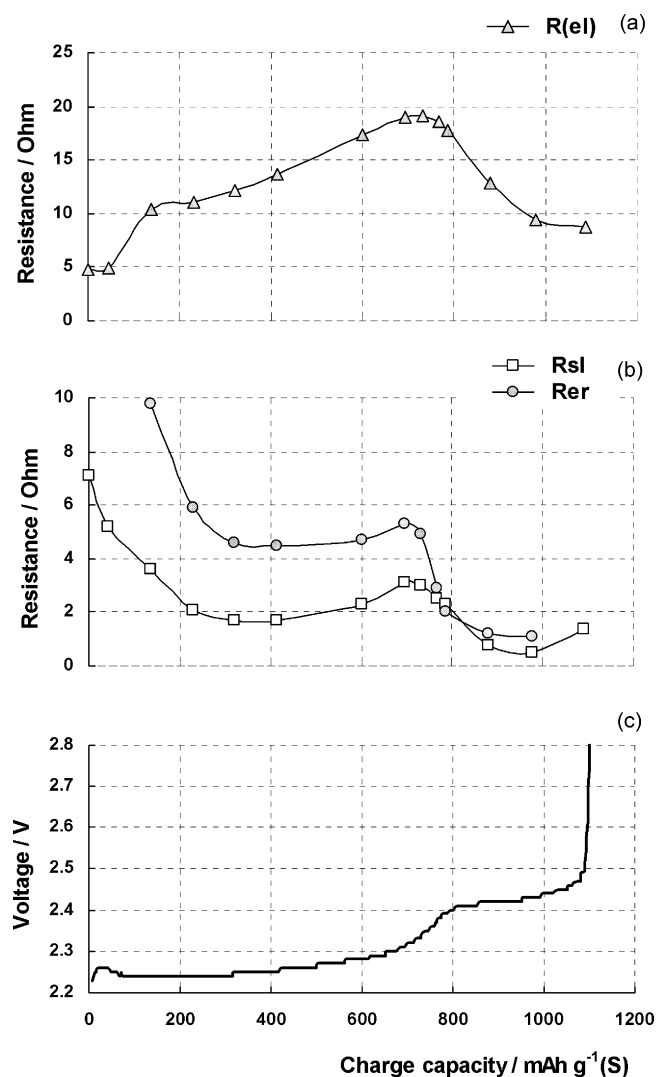
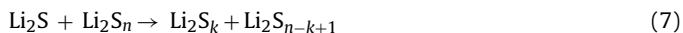


Fig. 7. The dependences of the electrolyte resistance (R_{el} , a), the resistance of the surface layers (R_{sl} , b) and the resistance to charge transfer (R_{er} , b) on the depth of charge of the two-electrode lithium-sulphur cell and the charge curve of the two-electrode lithium-sulphur cell (c). $i = 0.2 \text{ mA cm}^{-2}$; room temperature; 3rd cycle.

discharge (R_{el} , Fig. 6a) are similar. The position of the maximum on these curves corresponds to the cell state with maximum electrolyte viscosity.

The curves corresponding to the resistance of the surface layers (R_{sl}) and the resistance of charge transfer (R_{er}) during charge (Fig. 7b) have the S-shape. An initial decrease in R_{sl} and R_{er} is likely to be caused by the dissolution of lithium sulphide from the surface of the electrodes due to its reaction with long-chain lithium polysulphides (7) [4] and its electrochemical oxidation on the sulphur electrode (2):



The next increase in the resistance of the surface layers (R_{sl}) is most probably due to the decrease in the conductivity of the electrolyte, located in the porous surface layers of the lithium and sulphur electrodes. The decrease in the electroconductivity of the electrolyte is caused by the dissolution of the lithium polysulphides, formed at the beginning of discharge. As lithium polysulphides accumulate in the electrolyte, in the porous surface layers, the resistance of these layers increases. The subsequent decrease of R_{sl} is due to the increase in the conductivity of the electrolyte; itself caused by the decrease in Li_2S_n concentration.

The resistance-capacity plot for charge transfer (R_{er}) during charging is similar to the resistance-capacity plot for the surface layers (R_{sl}), Fig. 7b. As the resistance of the surface layers is determined by the resistance of the electrolyte located in their pores, this similarity indicates that the electrochemical processes which occur during the charging of a lithium-sulphur cell are controlled by the transport properties of the electrolyte system.

4. Conclusions

Impedance measurements made on lithium-sulphur cells, during cycling, show that the conductivity of the electrolyte changes because of the dissolution of lithium polysulphides. The properties of the electrolyte significantly influence the rates of the electrochemical processes which occur both on the sulphur and lithium electrodes.

Acknowledgment

This work was supported by Oxis Energy Ltd. (UK) under contract no. 17141/6-07.

References

- [1] R.D. Rauh, K.M. Abraham, G.F. Pearson, J.K. Surprenant, S.B. Brummer, J. Electrochem. Soc. 126 (1979) 523–527.
- [2] H. Yamin, E. Peled, J. Power Sources 9 (1983) 281–287.
- [3] H. Yamin, A. Gorenshstein, J. Penciner, Y. Sternberg, E. Peled, J. Electrochem. Soc. 135 (1988) 1045–1048.
- [4] V.S. Kolosnitsyn, E.V. Karaseva, Russ. J. Electrochem. 44 (2008) 506–509.
- [5] D.-R. Chang, S.-H. Lee, S.-W. Kim, H.-T. Kim, J. Power Sources 122 (2002) 452–460.
- [6] V.S. Kolosnitsyn, E.V. Kuzmina, E.V. Karaseva, ECS Trans. 25 (2009) 25–30.
- [7] URL: <http://www.scribner.com>.
- [8] V.S. Kolosnitsyn, E.V. Karaseva, A.L. Ivanov, Russ. J. Electrochem. 44 (2008) 564–569.
- [9] Y.-J. Choi, Y.-D. Chung, C.-Y. Baek, K.-W. Kim, H.-J. Ahn, J.-H. Ahn, J. Power Sources 184 (2008) 548–552.
- [10] H. Yamin, J. Penciner, A. Gorenshstein, M. Elam, E. Peled, J. Power Sources 14 (1985) 129–134.
- [11] Y. Li, H. Zhan, S. Liu, K. Huang, Y. Zhou, J. Power Sources 195 (2010) 2945–2949.
- [12] W. Zheng, Y.W. Liu, X.G. Hu, C.F. Zhang, Electrochim. Acta 51 (2006) 1330–1335.
- [13] J.H. Karchmer, The Analytical Chemistry of Sulfur and its Compounds, Part I, WILEY-INTERSCIENCE, New York, 1970, pp. 10–12.
- [14] H.-S. Ryu, H.-J. Ahn, K.-W. Kim, J.-H. Ahn, K.-K. Cho, T.-H. Nam, J.-U. Kim, G.-B. Cho, J. Power Sources 163 (2006) 201–206.